Sources and Mechanism of Degradation in P-type Thiophene-Based Organic Electrochemical Transistors

Emily A. Schafer[a,b], Ruiheng Wu[c], Dilara Meli[d], Joshua Tropp[a,b], Maximilian Moser[e,f], Iain McCulloch[e,f], Bryan D. Paulsen[a], Jonathan Rivnay[a,b]**

[a] Dept. of Biomedical Engineering, Northwestern University, Evanston, IL 60208

[b] Simpson Querrey Institute, Northwestern University, Chicago IL 60611

[c] Dept. of Chemistry, Northwestern University, Evanston, IL 60208

[d] Dept. of Materials Science and Engineering, Northwestern University, Evanston, IL 60208

[e] Dept. of Chemistry, Chemistry Research Laboratory, University of Oxford, Oxford, OX1 3TA, United Kingdom

[f] King Abdullah University of Science and Technology (KAUST), KAUST Solar Center, Thuwal, 23955-6900, Saudi Arabia

*Email: jrivnay@northwestern.edu, bryan.paulsen@northwestern.edu

Keywords: conjugated polymers, transistors, organic, stability, degradation

Abstract

Achieving high stability is critical for the implementation of organic electrochemical transistors (OECTs) in more diverse and demanding applications. However, the sources and mechanisms of OECT degradation have not been rigorously explored. Here, we employ a variety of biasing schemes to separate the relative effects of oxidative bias stress, reductive bias stress, and current stress on degradation of thiophene-based, p-type OECTs. We find that accelerated degradation arises from the compounding effects of simultaneous oxidative and reductive bias stress and is common across several thiophene-based channel materials. To understand the underlying mechanism of OECT channel degradation, we explore the individual contributions of dissolved oxygen and source-drain electrode materials. We determine that the reaction of dissolved oxygen at buried Au/OMIEC interface of the drain electrode experiencing reductive potentials produces a mobile reactive species that aggressively degrades the oxidized OMIEC throughout the device, destroying its conjugation and disrupting electronic charge transport. Importantly, we find that this mechanism can be disrupted by alternatively removing oxygen, avoiding reductive potentials in the device biasing scheme, replacing Au electrodes with a non-catalytic alternative, or passivating Au electrodes with self-assembled monolayers. These conclusions can inform both future standards of stability testing in the field as well as design considerations of OECT implementation in long-term applications.

Introduction

Conjugated polymers have great potential to meet new challenges in bioelectronic applications.[1,2] Of particular interest are organic mixed ionic-electronic conductors (OMIECs), a subset of conjugated materials that, in addition to their (semi)conducting properties, can take in and transport ions/water in a way that permits volumetric ionic-electronic charge coupling.[3] The resulting volumetric capacitance of OMIECs allows efficient interconversion of ionic and electronic signals across the biotic-abiotic interface.[4–6] In OMIECs implemented as the channel of organic electrochemical transistors (OECTs), this ionic-electronic coupling produces a doping effect that modulates electrical conductivity, enabling low-voltage, high-transconductance devices that can both sense and amplify biological signals.[7,8] The specific advantages of organic materials over traditional inorganic electronics, namely their synthetic tunability, bioinert/compatible nature, soft mechanical properties, and low electrochemical impedance, make these materials and OECTs highly attractive for biological bioelectronic interfacing. OECTs have therefore found success in ion and biomolecule sensing[9–12], cell impedance sensing[13,14], electrophysiology[15–17], electrical stimulation[18], and recently COVID-19 detection.[19,20] In order for OMIEC-based OECTs to realize their full potential in these applications and others, their implementation requires material stability that extends beyond the device lifetime and projected needs of the application. Degradation of the OMIEC channel in OECTs not only leads to diminished device performance over time, making calibration and use in long-term applications unattainable, but can also result in degradation products that may deleteriously affect both the device and surrounding tissue. For example, some OMIEC channel materials have been shown to produce reactive oxygen species from oxygen reduction reactions after long-term use,[21] which is known to cause oxidative stress in tissue and damage critical cellular structures.[22]

The stability of OECTs has been assessed through repetitive cycling or pulsing for a variety of OMIEC channel materials,[23–36] but non-standardized testing conditions (applied potentials, pulse times, sweep rates, total cycles) makes comparisons across studies difficult. Following the precision synthetic control of OMIEC chemical structure,[37,38] the most insightful investigations into OECT degradation to date have compared the *relative* stability of OMIECs with systematically varied molecular design.[37,39-55] However, for these studies to lead to broader rules for the design of OECT channel materials, investigations into the mechanisms of OMIEC degradation in OECTs are required.

Previous attempts to rigorously probe OMIEC electrochemical stability have focused on the redox stability of OMIEC-coated electrodes, which has then been correlated with OECT stability and degradation.[21,49,56] Functioning OECTs, on the other hand, present a more complicated environment than a uniform thin film. For one, the OMIEC in the channel of an OECT spans a distance between source and drain contacts (Figure 1a) and experiences a potential gradient due to the drain voltage (V_D) applied between the two contacts. Thus, while an OMIEC-coated electrode experiment uniformly modulates the potential of the OMIEC through oxidative and reductive environments, the bulk OMIEC layer in an OECT can experience both oxidative and reductive environments simultaneously as the potential of the gate (V_G) is modulated (Figure 1b-d). Adapting a concept from the broader transistor literature, the degradation induced by the various potentials throughout the OMIEC channel can be thought of as an electrochemical bias stress.[57,58] The potential gradient (electric field) between the source and drain electrodes drive currents (~ mA) through the OMIEC channel, leading to current densities often > 10^6 times larger than those arising from redox charging in the cycling of an OMIEC-coated electrode. Degradation induced by the current passing through the OMIEC channel can be defined as a current stress.

Current or bias stress-induced loss of redox activity within the OMIEC channel (loss of electronic charge carriers able to contribute to channel currents) is not the only source of OECT degradation. These stresses may also induce OECT performance degradation through the disruption of the macroscale percolative pathways necessary for charge transport across the OMIEC channel between the source and drain contacts.[56,59] The disruption of these transport pathways, whether morphological or chemical, could hinder transport of electronic charge carriers, leading to decreased channel current and transconductance and diminishing the ability to amplify signals. Besides degradation arising from disruption of macroscopic charge transport, current- and bias-stress may induce shifts in the device's threshold voltage and OFF currents that could also limit device utility in long-term applications.

To unravel these factors and identify the causes of accelerated OECT degradation, the cycling stability of a variety of p-type glycolated polythiophene OMIEC channel materials was studied in an array of biasing schemes selected to isolate the individual effects of current stress, oxidative bias stress, and reductive bias stress. These experiments revealed the particular electrochemical potential conditions that give rise to accelerated OECT degradation. Spectroelectrochemical experiments were carried out to further understand the specific mechanism of this degradation. The hypothesized chemical reaction deleterious to OMIEC stability appears to be electrode-dependent and possible reaction pathways for this degradation are discussed. Finally, practical materials, device fabrication, and OECT implementation schemes are presented that overcome accelerated OECT degradation. These insights are fruitful for informing OMIEC channel material development, OECT device architecture, and ultimate device implementation for next generation bioelectronics.

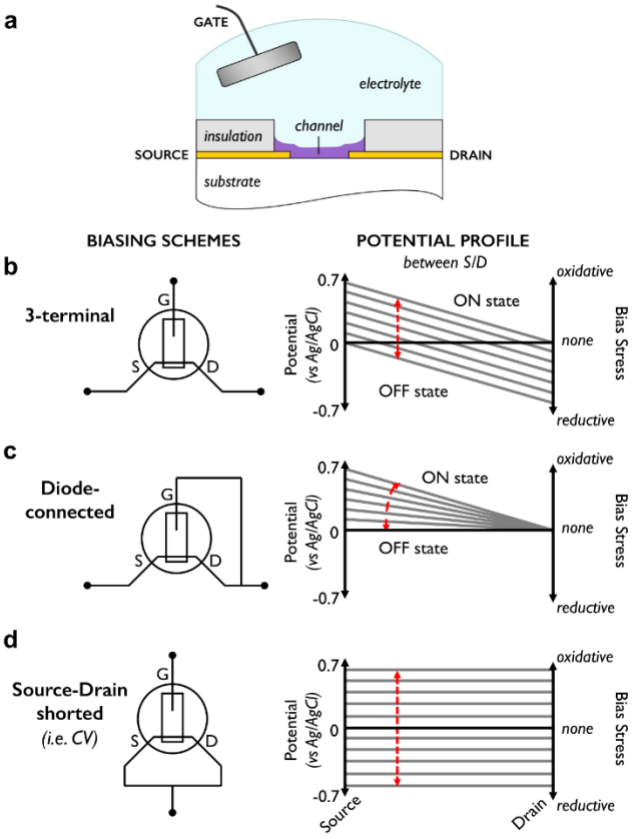

Figure 1. (a) Schematic of an organic electrochemical transistor (OECT) fabricated with gold source and drain contacts, a Ag/AgCl gate electrode, and an OMIEC channel, not to scale. Biasing scheme and resulting potential profile schematic across the OECT channel in the (b) three-terminal, (c) diode-connected, and (d) CV-like source-drain shorted biasing schemes. The electrochemical potentials (assumed here to vary linearly for clarity's sake) experienced by the channel are shown as a function of channel position, where the red arrow denotes the potential range at a particular V_D as V_G is swept during transfer curve cycling.

Experimental Section

OMIEC materials and solution preparation. P(g3T2-T)[60], and p(g2T-TT)[37] synthesis are reported elsewhere, p(g3T2-O) synthesis is reported in the Supporting Information. All polymers were individually dissolved at 5 mg/mL in $CHCl_3$ by stirring overnight at 40 °C.

OECT fabrication. Transistors were fabricated using a parylene-C peel-off method as previously reported.[61] Briefly, cleaned glass slides (1 in. × 3 in.) were spun with the negative photoresist AZ nLOF 2035 (MicroChemicals) at 3500 rpm for 30 s and baked at 110 °C for 120 s, followed by UV exposure using a SUSS MJB4 mask aligner and baked again at 110 °C for 120 s, then developed in AZ300MIF. The gold contacts and interconnects of 5 nm chromium/100 nm gold of the devices were deposited using an AJA E-beam system, and the subsequent lift-off was performed in acetone for 15 min. The 1.5 μm thick insulating layer of parylene-C was deposited (LabCoater II) with A-174 silane (Silquest) to promote surface adhesion. A thin layer of 2% soap solution (Micro90) was spun before the second 1.5 μm thick sacrificial layer of parylene-C was added. The two parylene-C layers were patterned and etched to expose the device active areas using the positive photoresist AZ P4620 spun at 3000rpm for 1 min and baked at 110 °C for 2 min. Substrates were then exposed to UV light using the mask aligner and developed in AZ400 K (1:4 dilution). Etching with a RAMCO reactive ion etcher was performed at 160 W with 50 sccm of O_2 and 10 sccm of CHF_3 for ~ 25 min until the gold contacts were revealed. The resulting transistors had channels of 100 μm x 10 μm in dimensions. These substrates were then plasma treated and spun with the 5 mg/mL solution of the OMIEC of interest (p(g3T2-O), p(g3T2-T), or p(g2T-TT)) in $CHCl_3$ at 1500 rpm for 45 s, then the sacrificial parylene-C layer was mechanically peeled off to pattern the polymer.

A comparison of OECT performance in devices with indium tin oxide (ITO) and gold contacts was performed on transistors 1 cm × 1 cm in area. For the gold contact transistors, the 1 mm width channel was patterned using a thin wire as a shadow mask in the E-beam system during metal deposition. For the ITO-contact transistors, ITO-coated glass slides (Nanocs, Inc.) were cleaned and spun with the positive photoresist S1813 (Shipley) at 4000 rpm for 30 s and baked at 115 °C

for 60 s. The wire was used as a mask when exposing the substrates to UV using the mask aligner and the slides were subsequently developed in AZ400K (1:4 dilution) for 60 s. The ITO was finally etched in a solution of 20% HCl and 5% nitric acid for 10 min and rinsed in deionized water and dried with N_2. Both the gold and ITO transistors with 1 mm channels were finally plasma treated and spun with the 5 mg/mL p(g3T2-O) solution according to the methods above.

For gold transistors with self-assembled monolayers, devices were fabricated and then incubated with a 2 mM solution of 6-mercapto-1-hexanol (Sigma-Aldrich) for 6 hours under darkness. The devices were rinsed with deionized water and spin-coated with p(g3T2-O) according to the methods above.

OECT stability testing. Transistors were tested in ambient using a potentiostat (Ivium) and recorded using IviumSoft. Each OECT first underwent four transfer curves in the diode-connected configuration with a scan rate of 250 mV/s to assure reproducible current-voltage behavior. OECTs tested in diode-connected, three-terminal, and S-D shorted (limited to either reductive cycling or oxidative cycling) were cycled 450 cycles over 30 minutes (Figure 1b-d), equivalent to 0.25 Hz cycling. For the three-terminal OECTs, a negative V_D was applied with respect to the drain electrode. OECTs tested in S-D shorted CV-like manner across the entire oxidative and reductive potential range were cycled for 225 cycles over 30 minutes to maintain a constant scan rate across OECTs of the same material. Scan rates were chosen such that devices operated well below their cutoff frequency ($\geq$ 100 Hz, as assessed by ON/OFF switching rise times), allowing the device channel ample time to fully charge and achieve its ON state with each cycle. The number of cycles was selected as to allow an adequate length of time to observe degradation in all of the materials tested. During cycling to assess the effects of scan rate on CV degradation, total number of scans were adjusted to keep a constant total amount of time cycled of 30 minutes. For devices cycled in

a low oxygen environment, p(g3T2-O) transistors of 100 µm x 10 µm dimensions were placed within a sealed chamber (Redox.me) containing approximately 10 ml of electrolyte that was sparged with hydrated N_2 for ~1 hour. In the resulting low oxygen aqueous environment, p(g3T2-O) transistors were then cycled following the same testing parameters described above. To compare electrode materials, cycling using the 1 mm channel length and 1 cm channel width transistors of gold and ITO contacts were performed in the three-terminal biasing scheme for 100 cycles with a scan rate of 150 mV/s. All measurements were taken using an Ag/AgCl pellet electrode (Warner Instruments) as the gate (equivalent to a combined reference and counter electrode) in a 0.1 M NaCl solution. Percent change in key metrics were reported after normalization to the devices' transfer curves before cycling, and all averages and standard deviations were calculated over at least three devices.

Spectroelectrochemistry. 1 × 3 cm^2 ITO coated glass (University Wafer) without and with 2 nm chromium/10 nm gold deposited via AJA E-beam system were cleaned via successive sonication in acetone and isopropyl alcohol and UV-ozone exposure, and p(g3T2-O) was spin-coated as above. Spectroelectrochemistry measurements of the substrates were carried out in 100 mM aqueous NaCl in a cuvette with an Ag/AgCl pellet (Warner Instruments) functioning as a combined counter and reference electrode. Potential control and current measurement were carried out with a potentiostat (Ivium). Simultaneous absorption spectroscopy was recorded with a halogen white light source (Ocean Optics, DH-2000-BAL) and an optical fiber light path split to separate UV-visible (Ocean Optics, FLAME-S) and near-infrared (Ocean Optics, NQ512) spectrometers, with 50 ms and 120 ms integration times, respectively. Electrochemical and spectroscopic data were recorded with IviumSoft and OceanView software, respectively. Data analysis, including the linecut and 2D color maps, was performed with MATLAB.

Raman spectroscopy. Raman measurements were performed using a HORIBA LabRam confocal microscope system. The excitation source was a HeNe laser (Melles Griot, 2.5mW) at 633 nm and a GaAlAs diode laser (Horiba, 450mW) at 785 nm. The laser beam was focused by an objective lens (× 50) and the focal point was carefully aligned onto the area of interest through the microscope. The beam size was smaller than 2 μm, determined through long time exposure (over 2 min). The data acquisition time for each frame was 1 s (for 633 nm) and 5 s (for 785nm), respectively, and then averaged over 10 frames. All data analysis and plotting was performed in MATLAB.

Atomic Force Microscopy (AFM). Scans of 5 μm × 5 μm dimensions were taken on substrates of ITO on glass, Au-coated glass, and Au-coated ITO on glass using a Dimension FastScan AFM instrument (Bruker) with a 3 Hz scan rate. Scans were analyzed using Nanoscope Analysis software to calculate the root-means-square surface roughness.

Grazing-incidence wide-angle x-ray scattering (GIWAXS). p(g3T2-O) was spin-coated onto Au-coated silicon wafers similar to above. Samples were cycled under one of three CV conditions: from 0 to +0.7 V, 0 to -0.7V, or from -0.7 to +0.7 V vs. Ag/AgCl. One sample was spin-coated onto bare silicon and left unbiased. GIWAXS data were collected at a photon energy of 10.9 keV at an incident angle of $\theta = 0.14°$ at Argonne National Lab's (ANL's) Advanced Photon Source (APS) sector 8-ID-E. Scattering patterns were analyzed using GIXSGUI and custom MATLAB scripts.

Dosing during electrochemical cycling. Cycling experiments were performed similar to the diode-connected biasing scheme reported above. For testing the effects of peroxides, small volumes of 1 mM H_2O_2 were pipetted into the electrolyte periodically throughout continuous cycling to increase the concentration of peroxides. For testing the effects of hydroxides, small

volumes of 100 µM NaOH were pipetted into the electrolyte in the same manner to reach a solution pH of 7.5, 8.0, 8.5, and 9.0.

Results and Discussion

In order to investigate the source and mechanism of degradation in OECTs, a model thiophene-based OMIEC material, poly(2,2'-(2-(3,3′-bis(2-(2-(2-methoxyethoxy)ethoxy)ethoxy))-bithiophene)-alt-2,5-furan) (p(g3T2-O)) (Figure 2a, inset), was first utilized to fabricate p-type OECTs and the corresponding devices were cycled in the saturation regime. This material was selected for its high performance and because it demonstrates moderate amounts of degradation within reasonable operating voltages, and therefore appeared to be a good representative material for degradations studies. Transfer curves before cycling of p(g3T2-O) OECTs with channel dimensions of 100 µm x 10 µm (Figure 2a) in aqueous 100 mM NaCl with a Ag/AgCl pellet gate electrode displayed negligible hysteresis, low threshold voltages (V_{Th} = 0.2 ± 0.04 mV), high drain current ($I_{D,max}$ = 206.1 ± 61 µA), and large gate transconductance (g_m = 0.724 ± 0.15 mS) at potential of +0.7 V vs Ag/AgCl (V_G = -0.7V). Upon ON/OFF cycling from 0 to +0.7 V vs Ag/AgCl with the drain held -0.7 V with respect to the source, the drain current dropped precipitously and began to trend towards a plateau in channel current after 450 cycles over 30 minutes (Figure 2b,c). In electrochemistry conventions, the working electrode potential (E) is generally reported versus a reference electrode or redox couple (e.g. V vs Ag/AgCl), whereas electrical engineering transistor formalism gate and drain electrode potentials (V_G, V_D) are referenced versus the grounded source electrode (V_S = GND = 0 V). For convenience's sake in relating OECT device performance to (spectro)electrochemistry data, we choose to present OECT current-voltage behavior (transfer curves) with the electrochemical convention of a potential (E) with respect to a

Ag/AgCl pellet gate electrode functioning as a combined reference and counter electrode. Thus, to convert between the two formalisms, $E = -V_G$.

OECT degradation was found not to be uniform across the channel when cycling these polythiophene-based transistors. Notably, swapping the source and drain connections on three-terminal biasing cycled p(g3T2-O) devices produced a moderate recovery of $I_{D,max}$ from 16% to 23.1% of the initial current of the pristine device, whereas p(g3T2-O) cycled using cyclic voltammetry (CV) resulted in no current recovery (Figure S1). Second, *ex situ* Raman spectroscopy on a similar thiophene based p-type polymer revealed chemical differences in the polymer near the source and drain after cycling (Figure S2). These observations cannot be explained by differences in OMIEC area overlaying the source and drain or OMIEC thickness across the channel. While not wholly unexpected, the non-uniformity of degradation serves as a reminder that OECT degradation is a more complex phenomenon than simple OMIEC redox cycling stability. Unlike in CV, the range of potentials experienced varies across the OECT channel during operation, with the channel near the drain undergoing a distinctly different potential cycling than the channel near the source. Degradation can then arise from current stress due to the source-to-drain current and bias stress cycling of potentials in the channel. The extent to which these factors contribute to OECT device degradation has not been previously explored and thus motivates further analysis of these p-type thiophene-based devices.

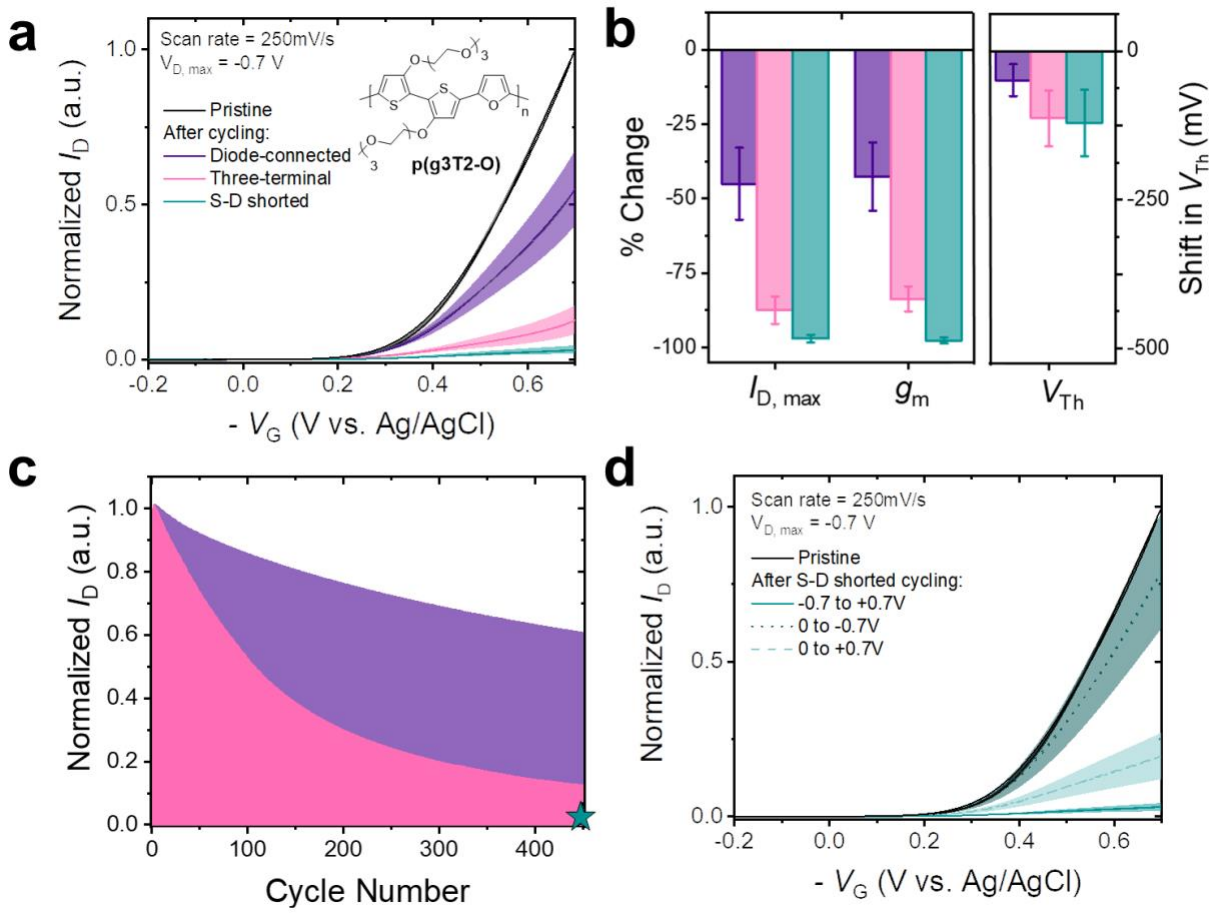

Figure 2. (a) Transfer curves of p(g3T2-O) (inset) before cycling (black) and after cycling for 30 minutes in diode-connected (purple), three-terminal (pink), and CV-like source-drain (S-D) shorted from -0.7 V to 0.7V (green) biasing schemes. Forward and reverse sweeps are shown with standard deviation for the forward sweep (n = 5). (b) Percent changes in $I_{D,max}$ and g_m and absolute shift in V_{Th} for the three-terminal, diode-connected, and S-D shorted biasing schemes. (c) Changes in $I_{D,max}$ over time across 450 cycles in diode-connected (purple) and three-terminal (pink) biasing schemes. The green star represents the final $I_{D,max}$ after cycling in S-D shorted biasing. (d) Transfer curves of p(g3T2-O) in diode-connected biasing scheme before cycling (black) and after cycling for 30 minutes in the S-D shorted, CV-like biasing from -0.7 V to +0.7 V vs Ag/AgCl (green, solid line), 0 to -0.7 V vs Ag/AgCl (dark green, dotted line), and 0 to +0.7 V vs Ag/AgCl (light green,

dashed line). Forward and reverse sweeps are shown with standard deviation for the forward sweep. All measurements were performed in 0.1 M NaCl with a Ag/AgCl pellet gate electrode.

Causes of OECT Degradation. To deconvolute the causes of degradation, OECTs cycled in different biasing schemes were compared, including the traditional three-terminal scheme, a drain-gate shorted diode-connected scheme, and a CV-like source-drain (S-D) shorted scheme (Figure 1). To collect OECT transfer curves in the traditional three-terminal biasing scheme, the potential between the source and Ag/AgCl gate electrodes was cycled (0 to +0.7 V vs Ag/AgCl) to switch the device between its OFF and ON states, while the drain electrode was kept at a fixed potential (-0.7 V) offset relative to the source to operate the OECT in the saturation regime. During cycling, the channel near the source contact alternated between neutral and oxidized (charge accumulated) state. The fixed potential offset of the drain electrode prevents charge accumulation in the channel near the drain, but also results in the channel near the drain contact experiencing a significant reductive potential when the source is in the OFF state (Figure 1b). The OMIEC channel therefore experiences a current stress from current transport across the channel, an oxidative bias stress in the channel near the source, and a reductive bias stress near the drain. After 450 cycles over 30 minutes in the three-terminal biasing scheme, an 87.4 ± 5% decrease in peak drain current, 83.6 ± 4% decrease in g_m, and a -0.11 ± 0.05 V absolute shift in V_{Th} were measured (Figure 2a,b). The cycling-induced shift in threshold, changes in device OFF currents were minor compared to the large decrease in channel current, which was the main contributor to the decrease in g_m.

In the diode-connected biasing scheme, the drain is no longer held at constant potential offset versus the source, but instead is shorted with the gate, and the potential of the shorted gate and drain is cycled to switch the device between the ON and OFF state (Figure 1c). As the potential is

swept, the OMIEC channel experiences a non-constant electrical field across the channel but always maintains saturation, thereby inducing an identical current stress to that of the three-terminal scheme. The OMIEC near the source undergoes the same oxidative bias stress (neutral when OFF, charge accumulation when ON), however the reductive bias stress of the channel near the drain electrode is absent, as the drain is always held at the same potential as the gate irrespective of ON or OFF state (Figure 1c). Simply, the diode-connected biasing scheme removes the effect of any reductive bias stress in the channel near the drain. Eliminating this reductive bias stress lessens the degradation by roughly half compared to the traditional three-terminal biasing scheme, resulting in only a 44.9 ± 12% decrease in peak current, 42.6 ± 11% decrease in g_m, and a smaller -0.05 ± 0.03 V shift in V_{Th} (Figure 2a,b). Compared to the traditional three-terminal scheme, the diode-connected device drain current decay over time was steady but less pronounced (Figure 2c). Swapping the source and drain contacts of the transistor after cycling still results in a recovery of the channel current from 45.1% to 51.9% of the initial current, indicating similar non-uniform degradation across the channel as in the three-terminal biasing scheme (Figure S1b).

To identify the effects of bias stress without an accompanying current stress, the cycling was repeated on OECTs with the source and drain shorted together in a CV-like biasing scheme. In this set-up, there is no significant channel current because of the lack of source-to-drain potential difference. Instead, the entire channel experiences the same bias stress as the channel is uniformly charged and discharged during cycling. The materials investigated exhibit high hole mobility (μ > 0.1 $cm^2\ V^{-1}\ s^{-1}$) such that in-plane charge transport is assumed not to impede the complete and uniform charging of the channel. The assumption of a uniformly charged channel is supported by spectroscopic mapping of charge density across similar materials and devices,[62,63] and is further confirmed as the extracted volumetric capacitances of OECT channels and more traditional

polymer coated electrodes were equivalent. V_G was cycled from -0.7 to +0.7 V to induce both the oxidative and reductive bias stress present in the three-terminal biasing scheme. Cycling in S-D shorted biasing followed by transfer curve measurements resulted in a nearly complete loss of channel current, with 96.3 ± 1.3% decrease in peak current, 97.6 ± 1% decrease in g_m, and a -0.012 ± 0.06 V shift in V_{Th} (Figure 2a-c).

The S-D shorted biasing scheme was also employed to probe the oxidative and reductive bias stresses independently and thereby mimic the individual contributions to degradation of the channel near the source and drain contacts, respectively, in the three-terminal biasing scheme. Reductive cycling alone from 0 to -0.7 V (mimicking the conditions in the channel near the drain electrode) induced a modest 20.6 ± 19% decrease in peak drain current, while oxidative cycling alone from 0 to +0.7 V (mimicking the conditions in the channel near the source electrode) induced a greater 80.4 ± 7% decrease in peak drain current (Figure 2d). Coincidentally, the drain current losses in the separate reductive and oxidative bias stress degradation sum to ~100%, roughly the equivalent to the 96.3 ± 1.3% decrease observed in combined -0.7 to +0.7 V cycling that induced both the oxidative and reductive bias stress. While this suggested a possible additive effect of OECT degradation, separate reductive and oxidative bias stress degradation summed to much less than the degradation induced in combined reductive and oxidative bias stress cycling, as discussed below.

These cycling experiments made clear that current stress is not the main contributor to device degradation. S-D shorted oxidatively-cycled (0 to +0.7 V vs Ag/AgCl) devices lacking any current stress did not show less degradation (which would be expected if current stress dominated), but instead displayed greater degradation than diode-connected devices, as now the whole channel experienced oxidative potentials, rather just than the channel region near the source (Figure 2a,d).

Further, while the three-terminal biased devices (experiencing both reductive and oxidative bias stress) degraded more rapidly than the diode-connected devices, it was not solely the reductive bias stress alone (present in the channel near the drain electrode in the three-terminal scheme) that induced the greater degradation, as the S-D shorted, reductively-cycled devices showed the least degradation (Figure 2d). The combination of both reductive and oxidative bias stress was therefore identified to be the apparent source of accelerated degradation, even if spatially separated (near the drain and source, respectively) across the OECT channel.

While the primary source of the degradation was identified as a combination of oxidative and reductive bias stress, the exact mechanism by which this occurs was less straightforward. Interestingly, the combined oxidative and reductive bias stresses did not induce current-voltage hysteresis or significant shifts in V_{Th} for all biasing schemes (Figure 2b). Further, none of the biasing schemes produced catastrophic delamination of the OMIEC channel, as optical micrographs evidenced no delamination of the films (Figure S3). As oxidation of OMIECs is known to induce swelling in electrolyte, one possible physical mechanism of degradation may arise from repetitive swelling and deswelling that occurs with cycling, with disruption accumulating cycle-by-cycle[52,64]. To examine this, we compared the scan rate dependence of degradation across cycling experiments such that while the number of cycles varied, the total time the channel spent at any given potential was the same. While increased scan rate (increased number of cycles) did marginally increase degradation, all scan rates displayed >90% decrease in $I_{D,max}$ (Figure S4). This reveals that the total time the device experiences bias stress, rather than the number of cycles it undergoes, has the largest effect on stability, meaning that the cumulative disruption from repetitive cyclic swelling and deswelling in the aqueous electrolyte is not the most

important mechanism of degradation. This has important implications on our understanding of OECT degradation, where stability is most often assessed via cyclic sweeping or pulsing.

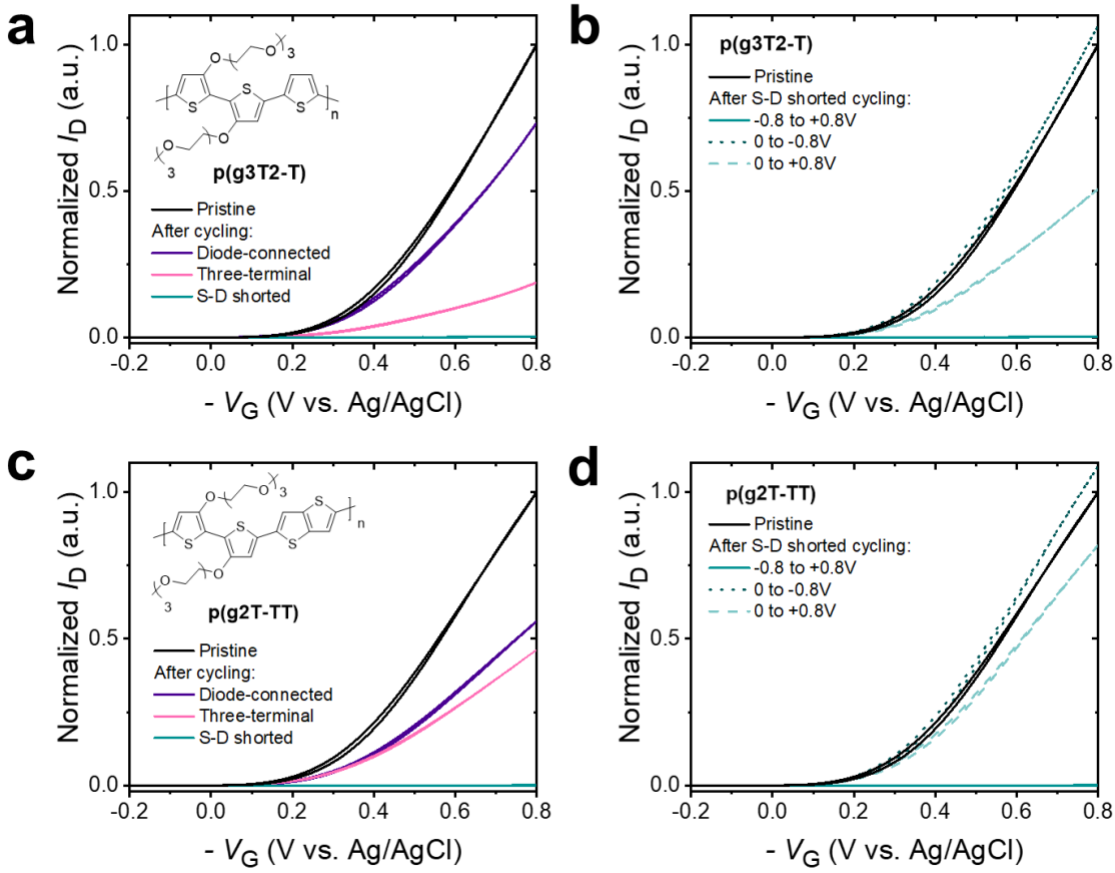

Figure 3. (a) Transfer curves of p(g3T2-T) (inset) before cycling (black) and after cycling for 30 minutes in diode-connected (purple), three-terminal (pink), and S-D shorted from -0.8 V to +0.8 V (green) biasing schemes. (b) Transfer curves of p(g3T2-T) in biasing scheme before cycling (black) and after cycling for 30 minutes in the S-D shorted, CV-like biasing scheme from -0.8 V to +0.8 V (green, solid line), 0 to -0.8 V (dark green, dotted line), and 0 to +0.8 V (light green, dashed line). (c) Transfer curves of p(g2T-TT) (inset) before cycling (black) and after cycling for 30 minutes in diode-connected (purple), three-terminal (pink), and S-D shorted from -0.8 V to +0.8

V (green) biasing schemes. (d) Transfer curves of p(g2T-TT) in biasing scheme before cycling (black) and after cycling for 30 minutes in the S-D shorted, CV-like biasing scheme from -0.8 V to +0.8 V (green, solid line), 0 to -0.8 V (dark green, dotted line), and 0 to +0.8 V (light green, dashed line). All measurements were performed in 0.1 M NaCl with a Ag/AgCl pellet gate electrode.

Generalizability of OECT Degradation. Due to the ubiquity of polythiophene-based channel materials for p-type accumulation-mode OECTs, cycling experiments were repeated with two other previously reported, high-performing polythiophene base p-type OMIECs to demonstrate the generalizability of these identified OECT degradation phenomena. The alternating block copolymers poly-3,3'-bis(2-(2-(2-methoxyethoxy)ethoxy)ethoxy)-2,2':5',2"-terthiophene (p(g3T2-T))[60,64] (Figure 3a, inset) and poly(2-(3,3′-bis(2-(2-(2-methoxyethoxy)ethoxy)ethoxy)-[2,2'-bithiophen]-5-yl)thieno[3,2-*b*]thiophene) (p(g2T-TT))[37] (Figure 3c, inset) were incorporated as the channels of OECTs, where the furan structural unit within the p(g3T2-O) backbone is supplanted with a an unsubstituted thiophene and thienothiophene, respectively. Both materials display high volumetric capacitance and hole mobility yielding high-gain OECTs.[37] As with p(g3T2-O), these OECTs were cycled to the limits of device stability (up to +0.8 V vs Ag/AgCl in this case) for 30 minutes in a three-terminal, diode-connected, and S-D shorted biasing scheme. Both of these materials demonstrated similar qualitative trends to p(g3T2-O), where the diode-connected biasing scheme induced the least degradation, followed by three-terminal biasing scheme, and the S-D shorted biasing caused a near complete suppression of channel transconductance (Figure 3a,c).

Individually assessing the effects of reductive and oxidative bias stresses in the S-D shorted biasing scheme again showed isolated reductive bias stress to have the least impact (Figure 3b,d). While p(g3T2-O) displayed a modest ~ 20% degradation after cycling from 0 to -0.7 V vs Ag/AgCl, p(g3T2-T) and p(g2T-TT) both showed slight increases in $I_{D,max}$, indicating a beneficial break-in process with isolated reductive bias stress. However, isolated oxidative bias stress still led to degradation in both p(g3T2-T) and p(g2T-TT). In p(g3T2-T), isolated oxidative bias stress cycling induced greater degradation than diode-connected cycling, similar to p(g3T2-O). The inverse was true for p(g2T-TT), with the S-D shorted cycling in oxidative potentials (0 to +0.7 V vs Ag/AgCl) degrading less than the diode-connected cycling, indicating current stress does contribute to degradation in this polymer. Nonetheless, concurrent oxidative and reductive bias stress was still the largest factor accelerating degradation (Figure 3b,d). These results indicate that the main drivers of OECT degradation are generalizable to polythiophene-based p-type accumulation-mode OMIECs. Whether these insights can be extended to OMIECs of other conjugated backbones and n-type conjugated polymers has yet to be evaluated and is worthy of future study.

After finding these broader trends in stability to be generalizable across other polythiophene OMIECs, we hypothesize that the degradation mechanism is an irreversible electrochemical reaction of these polymers arising from the concurrent reductive and oxidative bias stresses. Remembering that accelerated degradation occurs even when the oxidative and reductive bias stress environments are spatially separated at opposite ends of the OECT channel, it would appear that accelerated degradation involves the mass transport of some reactive species between the reductive (near the drain) and oxidative (near the source) bias stress environments. We speculate that this species is produced near the drain and is deleterious to the oxidized polymer near the

source. With these experiments allowing us to pinpoint the dominant source of accelerated OECT degradation, we now interrogate the mechanisms of this degradation to detail its direct effects on the OMIEC in question.

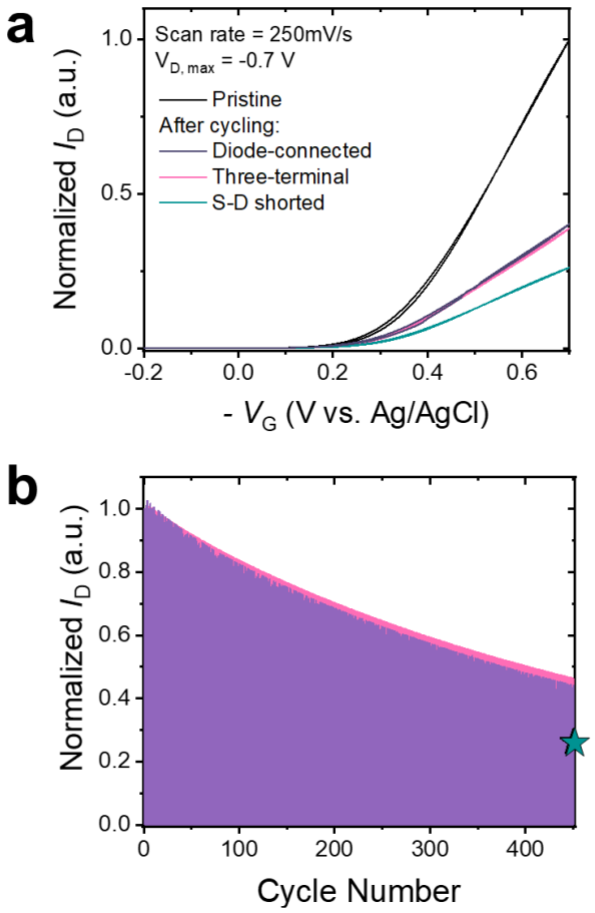

Figure 4. (a) Transfer curves of p(g3T2-O) in low oxygen conditions before (black) and after cycling for 30 minutes in diode-connected (purple), three-terminal (pink), and CV-like source-drain (S-D) shorted from -0.7 V to +0.7 V vs Ag/AgCl (green) biasing schemes. (b) Changes in $I_{D,max}$ over time across 450 cycles in diode-connected (purple) and three-terminal (pink) biasing schemes. The green star represents the final $I_{D,max}$ after cycling in S-D shorted biasing from -0.7 to +0.7 V vs Ag/AgCl.

Electrochemical Mechanisms of OECT Degradation. Oxygen is generally presumed to play an important role in degradation of organic electronic devices. To confirm this, device cycling experiments in the various biasing schemes were repeated for p(g3T2-O) OECTs in a low oxygen (O_2) environment. Low O_2 cycling in the diode-connected biasing scheme lead to equivalent degradation compared to diode-connected cycling in ambient conditions (low O_2 $I_{D,max}$ after 30 minutes of cycling within ~1 standard deviation of the average degradation in $I_{D,max}$ in ambient) (Figure 4). Strikingly, when cycled in a low O_2 environment, degradation of three-terminal biased devices was limited so that three-terminal and diode-connected devices showed no difference in degradation (Figure 4). This indicates that the accelerated degradation induced by the presence of a reductive bias stress at the drain electrode is completely dependent on the presence of oxygen. Similarly, the stability of S-D shorted devices cycled in a CV-like manner from -0.7 to +0.7 V vs Ag/AgCl was markedly improved in a low O_2 environment ($I_{D,max}$ decrease of 73.8% in a low O_2 environment compared to 96.3% in ambient).

To probe the redox behavior of the oxygen-related mobile species that accelerates degradation, CV on p(g3T2-O) OECT channels with a staircase potential profile and a delayed current measurement were employed to resolve the faradaic electrochemical processes from the large (pseudo)capacitive charging currents. In the presence of ambient oxygen, cyclic voltammograms on S-D shorted devices from -0.7 to +0.7 V vs Ag/AgCl showed the growth of a forward oxidation and reverse reduction waves with successive cycling, indicating the buildup of a redox species with cycling (Figure S5a). When repeated on similar p(g3T2-O) OECT channels in a N_2 sparged, low O_2 environment, the measured faradaic currents were below the noise level (Figure S5b). This

demonstrated that ambient oxygen leads to the production of a dissolved redox active species, which was suspected of accelerating the degradation of the OECT channel material.

Ambient spectroelectrochemistry on p(g3T2-O) thin films was performed to further elucidate the suspected O_2-induced electrochemical mechanism of OECT degradation. In order to accurately reflect the materials, structure, and environment of a functioning OECT, spectroelectrochemistry was carried out on ITO substrates coated with a continuous Au film (standing in for the Au source or drain electrode) on ITO. The Au coating was sufficiently thin (~10 nm) such that it was adequately transparent for transmission mode UV-Vis-NIR. Atomic force microscopy (AFM) revealed the Au-coated ITO showed no increase in surface roughness (Figure S6), indicating a continuous film coating. Electrochemical cycling was carried out with a true linear analog sweep generator to ensure accurate measurement of the (pseudo)capacitive charging currents. When cycled from potentials reflecting the OECT OFF and ON states, the absorption spectra transitions from a strong neutral π-π* absorption around 575 nm in the OFF state, which in the ON state is bleached, with polaronic absorptions (centered around 1070 nm) and bipolaronic absorptions (centered around 1280 nm) arising, representing the presence of charged species (holes) on the polymer backbone (Figure S7).

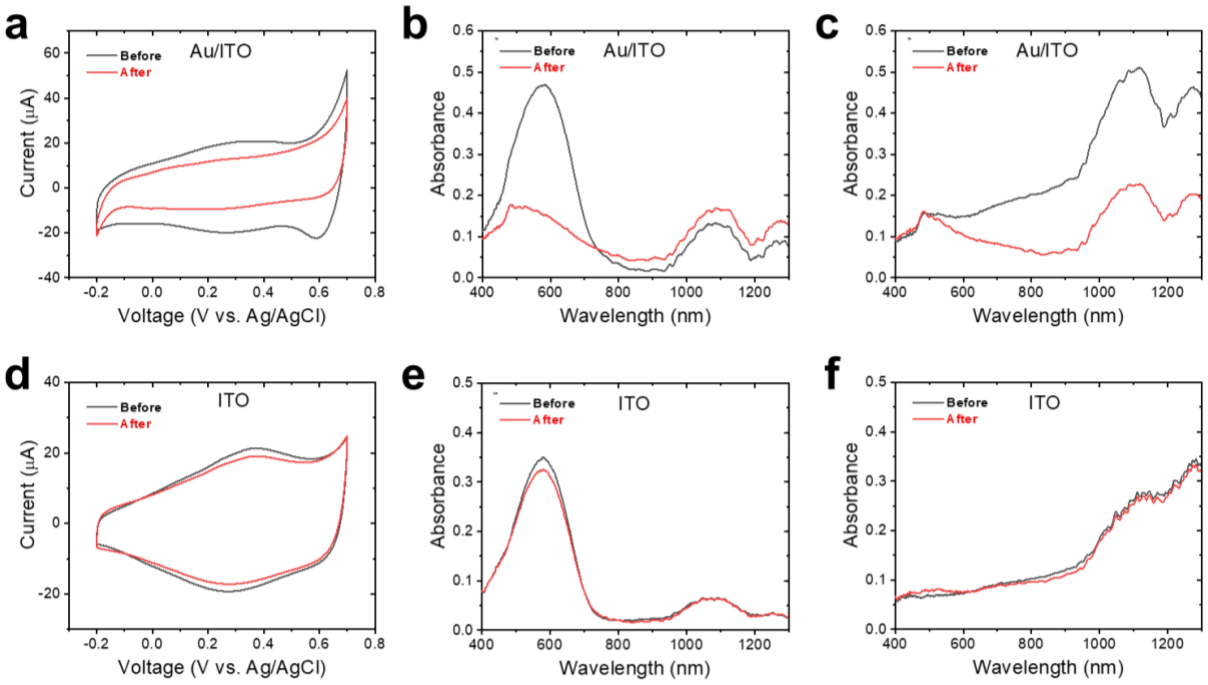

Figure 5. (a) CV of p(g3T2-O) before (black) and after (red) cycling from -0.7 to +0.7 V on Au-coated ITO substrates. UV–Vis–NIR spectra before and after cycling from -0.7 to +0.7 V on Au-coated ITO substrates under (b) OFF state (-0.7 V vs Ag/AgCl) and (c) ON state (+0.7 V vs Ag/AgCl). (d) CV of p(g3T2-O) before (black) and after (red) cycling from -0.7 to +0.7 V on ITO. UV–Vis–NIR spectra before and after cycling from -0.7 to +0.7 V on ITO under (e) OFF state (-0.7 V vs Ag/AgCl) and (f) ON state (+0.7 V vs Ag/AgCl). All measurements were performed in 0.1 M NaCl with a Ag/AgCl pellet gate electrode.

Similar to the above OECT characterization shown in Figure 2, films on Au/ITO were cycled for 30 minutes from 0 to +0.7 V vs Ag/AgCl to mimic the oxidative bias stress which occurs in the channel near/at the source, from 0 to -0.7 V vs Ag/AgCl to mimic the reductive bias stress which occurs in the channel near/at the drain, and from -0.7 to +0.7 V vs Ag/AgCl to capture the combined effect of both oxidative and reductive bias stresses. Oxidative cycling alone (0 to +0.7

V vs Ag/AgCl) produced minimal changes in the cyclic voltammograms, showing only a slight decrease in current levels indicating a marginal loss of capacity, and the strength of the neutral and polaronic absorptions were retained in the OFF and ON states respectively (Figure S8a-c, S9c,d). The reversible bleaching of the absorption features with electrochemical cycling was also similarly maintained.

Reductive cycling alone (0 to -0.7 V vs Ag/AgCl) on Au/ITO significantly changed the shape of the cyclic voltammogram, and the final solution was found to be shifted basic (pH = 8.5) (Figure S8d). This is in contrast to the aqueous solution collected after oxidative cycling, which was found to still be roughly neutral in pH. However, these changes did not manifest in the spectral data as the strength of the neutral and polaronic absorptions were retained in the OFF and ON states, respectively, as were the reversible bleaching of the absorption features with electrochemical cycling (Figure S8e,f, S9e,f). The change in CV shape was attributed to the change in pH with cycling, as CVs collected on pristine p(g3T2-O) films with the used basic electrolyte demonstrated immediate loss of current reflective of degradation that stopped after switching to fresh pH neutral electrolyte (Figure S10). The shift in pH implies that although there is no significant pseudocapacitive charging of the polymer film in this region, nonetheless there is some species being produced, likely faradaically.

Cycling across the entire range (-0.7 to +0.7 V vs Ag/AgCl) on Au/ITO also shifted the solution pH basic (pH = 8.5). However, when cycling across both the oxidative and reductive bias stress ranges, large and irreversible changes were observed in both the CVs and the potential-dependent spectra. The CV current levels decreased significantly and flattened, losing features indicative of charging and discharging (Figure 5a). Additionally, the neutral π-π^* and charged (bi)polaronic absorptions were greatly diminished in the OFF and ON states, respectively (Figure 5b,c, S9a,b).

This reflected a permanent loss of most of the ordered conjugated chromophores on the p(g3T2-O) backbone, which understandably accompanies a loss of capacity and electrical conductivity, as seen in the above OECT studies (Figure 2a). The irreversible degradation process during electrochemical cycling as recorded by the spectroelectrochemistry implied that degradation was most severe in the ordered regions of the OMIEC, as the neutral absorptions associated with the amorphous regions (495 nm), while greatly suppressed, still degraded less compared to the more ordered aggregates (575 nm) (Figure S11). This also manifests as a loss of structural order of the polymer, as assessed by grazing-incidence wide-angle x-ray scattering (GIWAXS) (Figure S12). Films of p(g3T2-O) on Au-coated silicon substrates that underwent *ex situ* reductive and oxidative bias stress cycling showed a clear expansion and contraction of their π-stack distance, respectively, as observed in previous structural analysis of other conjugated polymers.[65–67] However, films cycled the entire range (-0.7 to +0.7 V vs Ag/AgCl) displayed a complete absence of π-stacking, consistent with a loss of aggregated conjugated backbones (Figure S12).

While the O_2-induced, (electro)chemical degradation of a π-conjugated system as the general mechanism of OMIEC-based OECT degradation seems like a trivial result, this degradation was surprisingly not present in the absence of Au. Repeating the above spectroelectrochemical experiments with p(g3T2-O) on ITO alone showed no obvious signs of degradation. In all three cases, (oxidative bias stress, 0 to +0.7 V vs Ag/AgCl; reductive bias stress, 0 to -0.7 V vs Ag/AgCl; both oxidative and reductive bias stress, -0.7 to +0.7 V vs Ag/AgCl) the CVs showed minimal capacity loss and strong neutral and bipolaronic absorptions were retained in the OFF and ON states, respectively, as were the reversible bleaching of the absorption features with electrochemical cycling (Figure 5d-f, S13, S14). Films on both the ITO and Au/ITO electrodes showed persistent (bi)polaronic absorptions when potentiostatically held in the OFF state (-0.7 V

vs Ag/AgCl) before and after multi-cycling experiments (Figure 5b,e). This indicates the persistent presence of charge in the film that either was unable to be extracted or was induced through ambient oxygen doping. However, presence of these (bi)polaronic absorptions in the OFF state after cycling in films on Au-coated ITO (where all other absorptions were greatly quenched) indicated that the chromophores associated with this charge persisting in the film were not affected by material degradation. Interestingly, with ITO electrodes, neither the 0 to -0.7 vs Ag/AgCl nor the -0.7 to +0.7 V vs Ag/AgCl cycling induced a basic pH shift in the aqueous electrolyte that was observed in the experiments employing of Au-coated electrodes.

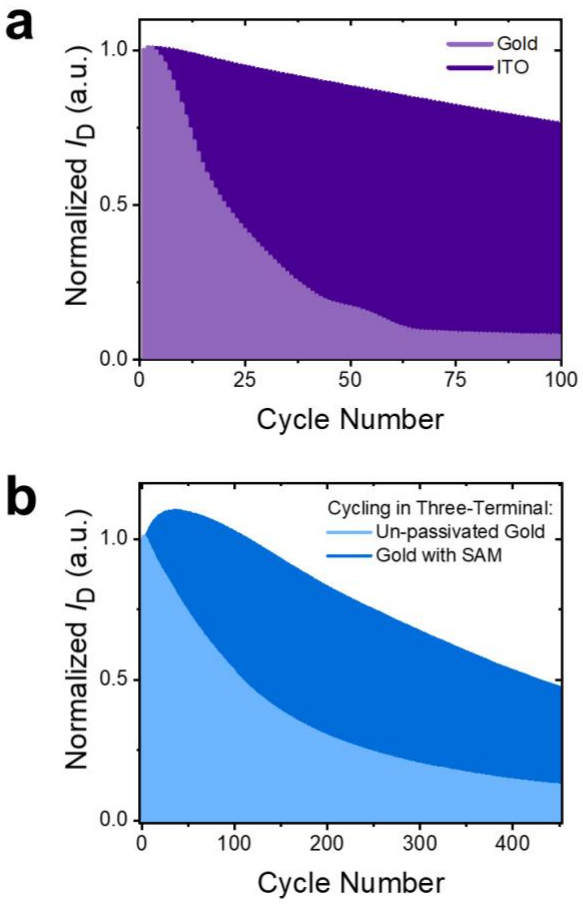

Figure 6. (a) Cycling of p(g3T2-O) over time in the three-terminal biasing scheme using

transistors with ITO (dark purple) and Au (light purple) contacts with a scan rate of 150 mV/s. (b) Cycling of p(g3T2-O) in the three-terminal biasing scheme using transistors with un-passivated Au source and drain contacts (light blue) and Au functionalized with an MCH SAM (dark blue). All measurements were performed in 0.1 M NaCl with a Ag/AgCl pellet gate electrode.

To determine if this observed electrode effects in spectroelectrochemistry were in fact the source of OECT degradation, devices with ITO source and drain contacts were fabricated and tested. Comparing OECTs with identical geometries fabricated with source/drain contacts from Au and ITO revealed a pronounced difference in OECT degradation (Figure 6a). OECT cycling in the traditional three-terminal biasing scheme with Au source/drain contacts showed a precipitous drop in $I_{D,max}$ leading to a plateau of less than 10% of the pristine device value, with a total 92.4% decrease over 100 cycles. Performance deteriorated to an $I_{D,max}$ below 200 μA and exhibited a large amounts of hysteresis by the final cycles. Cycling comparable OECTs with ITO source/drain contacts showed a much more gradual decay in $I_{D,max}$ and resulted in only a 23.9% decrease over 100 cycles (Figure 6a). Thus, the electrochemical behavior of the source-drain electrode material appears to dictate the overall degradation of the device, rather than purely the properties of the OMIEC channel material. The use of gold as the source/drain contacts has an obvious role in the primary mechanisms of accelerated OECT degradation measured during cycling. Further, the large differences between the OECT behavior using gold and ITO contacts demonstrates that studying future OMIEC stability on ITO during spectroelectrochemistry is not reflective of actual degradation behavior in OECTs that commonly use Au source and drain electrodes.

To further probe the role of gold electrode interface in accelerated device degradation, OECTs were fabricated with a self-assembled monolayer (SAM) passivation layer formed on the gold

source and drain contacts before depositing the OMIEC. The addition of a SAM of 6-mercapto-1-hexanol (MCH) allowed charge injection/collection from the gold to the OMIEC to occur, but minimized the adsorption of the OMIEC or other species directly on the gold surface. When these OECTs were tested under the same conditions, pristine transfer curves still demonstrate similarly ideal transistor behavior with only a slight shift in threshold voltage compared to un-passivated gold (V_{Th} = 0.19 ± 0.01 V) (Figure S15a). Cycling in the three-terminal biasing scheme led to a decrease in $I_{D,max}$ of only 55% over 30 minutes compared to the nearly 90% drop in devices lacking the SAM (Figure 6b, S15b). On the other hand, the difference in device performance after diode-connected cycling between the uncoated and SAM-coated gold transistors was extremely small (Figure S15c). In fact, SAM-coated devices cycled in the three-terminal biasing scheme (experiencing both reductive and oxidative bias stress) underwent degradation equivalent to the diode-connected devices (only experiencing oxidative bias stress) (Figure S15d). We therefore conclude that the SAM successfully inhibits the reductive bias stress driven reaction that accelerates OECT degradation, and that the remaining degradation of the three-terminal cycled device is predominantly from the oxidative bias stress alone, as in the diode-connected cycled device.

Identity of Reactive Species. These experiments offer a clearer picture of the sources and mechanisms of OECT degradation for thiophene-based OMIECs, yet the exact mobile reactive species produced at the buried Au/OMIEC interface experiencing reductive potentials, which is responsible for accelerated degradation, is still unknown. Due to the basic pH shift in the cycling conditions that induced degradation and the dependence of degradation on oxygen, the presence of hydroxide was identified as a possible cause. To definitively determine if hydroxide could cause OECT degradation, transistors operating in the diode-connected biasing scheme were dosed with

successively higher concentrations of aqueous NaOH solution over time. The diode-connected scheme does not produce the chemically active species from reductive bias stress, so if hydroxide ions are the causative agent of degradation, dosing the electrolyte during cycling should then cause device performance to mimic the degradation during cycling in three-terminal biasing. However, no changes in the rate of degradation were observed throughout cycling despite reaching a pH of 9, in excess of the pH measured in cycling experiments (Figure S16a). Thus, while hydroxide may be a side product of the degradation reaction, it was ruled out as mobile reactive species directly causing accelerated OECT degradation.

Hydrogen peroxide was also identified as a possible chemical species responsible for the electrochemical degradation. Electrochemical side reactions with oxygen to produce hydrogen peroxide have previously been implicated as a sources of OECT instability,[21] and similar OMIEC materials have even been employed as electrodes in the electrocatalytic production of hydrogen peroxide. Hydrogen peroxide produced during cycling could in turn react with and degrade the neutral or oxidized polymer. However, standard peroxide test strips (MilliporeSigma 1.10081.0001 MQuant) and commercial electrochemical hydrogen peroxide sensors (Innovative Instruments, Inc.) showed no measurable production of hydrogen peroxide during cycling, with a limit of detection of 0.3 mM and 1 μM, respectively. To definitively determine if hydrogen peroxide could cause OECT degradation, transistors operating in the diode-connected biasing scheme were dosed with successively larger amounts of hydrogen peroxide over time. No changes in the rate of degradation were observed throughout cycling despite reaching a peak hydrogen peroxide concentration of 100 μM (Figure S16b). Consequently, hydrogen peroxide was found to neither be produced in any significant quantity nor to be the mobile reactive species responsible for accelerated OECT degradation.

Converting the applied potentials from V vs Ag/AgCl to V vs RHE, the potentials in our devices range from roughly -0.09 to +1.31 V vs NHE in the pH ~ 7 condition (during cycling that lacks a reductive bias) and from roughly 0.00 to +1.40 V vs NHE in the pH ~ 8.5 condition (during cycling that produces a reductive bias). p(g3T2-O) is oxidized above ~0.4 V vs NHE (-0.3 V vs Ag/AgCl), and Au and ITO electrodes are expected to be electrochemically stable across these potentials.[68] In these potential ranges, the two- and four-electron oxygen reduction reaction (ORR) pathways of dissolved ambient oxygen are thermodynamically possible, which may account for the OH^- production during reductive bias stress. However, as shown with both peroxide and hydroxide dosing experiments, these products of the two- or four-electron ORR, respectively, are not the mobile chemical species responsible for accelerated OECT degradation. Still, ORR-produced reactive oxygen species, such as the superoxide, may be the species responsible for accelerated degradation.[69]

In addition, no visible evidence of gas evolution was observed during experiments. This was reasonable because although the total range of potentials reached spanned 1.4 V, the maximum potential difference between electrodes within the device at any given moment was 0.7 V. This precluded direct water splitting and eliminated evolved hydrogen gas as the mobile reactive species. Carbon oxidation is also thermodynamically feasible, but such reactions would be expected to shift the solution pH more acidic through the formation of carbonic acid, whereas the opposite pH trend was observed.

When considering the potential degradation reactions induced by mobile chemical species, the reduced aromaticity and increased reactivity of the furan repeat unit[70] is not suspected to be the ultimate source of accelerated degradation as the same trends are observed in furan-free polymers. The thiophene structural units may be susceptible to oxidative conversion into corresponding

sulfones and sulfoxide derivatives, a behavior observed in other conjugated polymer-based electrodes.[71] While such oxidation could explain the observed permanent loss of conjugation observed in the spectroelectrochemical experiments, such oxidation generally requires low-pH environments or H_2O_2,[72] both of which have been systematically ruled out and are independent of the electrode identity. A possible candidate for degradation chemistry may be C-S bond scission of thiophenes adsorbed on Au surfaces,[73] which may explain the contribution of bare Au electrodes in accelerating degradation, though how this would affect the film beyond the Au/polymer interface is not clear. Thus, the identity of the mobile reactive species and its particular chemistry that accelerates OECT degradation remains unclear and should be the topic of future investigation.

Conclusion

Stability of OECT performance is a critical device requirement for use in long-term applications such as biological interfacing, yet the sources and mechanisms of OECT degradation have not been comprehensively studied. With combined cycling studies of OECTs in different biasing schemes and their corresponding spectroelectrochemical analysis, we isolated the factors contributing to device degradation and identified which have the greatest influence on OECT stability. While current stress and oxidative bias stress are unavoidable in p-type OECTs, these experiments show that accelerated OECT degradation is driven by a compounding effect of reductive and oxidative bias stress occurring in the presence of oxygen and un-passivated Au electrodes. This accelerated degradation follows the general mechanism of dissolved oxygen reacting at buried Au/OMIEC interface at the drain electrode experiencing reductive potentials to produce mobile reactive species that aggressively degrades the oxidized OMIEC throughout the device, disrupting its conjugation and destroying its electronic charge transport properties.

In detailing this mechanism, possible routes to decrease OECT degradation and improve stability become apparent. The mechanism of accelerated degradation can be disrupted by removing oxygen, avoiding reductive potentials in the device biasing scheme, or avoiding the use of un-passivated Au electrodes. While operating in oxygen-free environments is likely infeasible in many applications, degradation can be slowed by lessening or removing the reductive bias stress itself. One strategy is to consider alternative biasing schemes, such as diode-connected OECTs that avoid reductive bias stress completely. Alternatively, OMIECs with deeper highest occupied molecular orbital (HOMO) could be employed as OECT channel materials. The deeper HOMO manifests in a larger V_{Th}, which then requires a smaller magnitude of V_D to reach the saturation regime. A smaller drain offset minimizes the reductive bias stress near the drain while operating in a traditional three-terminal biasing scheme. A similar approach has been applied to avoid spontaneous oxygen doping.[21] Un-passivated Au source and drain contacts can be avoided by choosing alternative electrode materials (such as ITO) or by passivating Au electrodes (such as with SAMs), which functions to inhibit the reaction of dissolved oxygen that gives rise to accelerated degradation. These material, device, and implementation considerations should be considered in future design of OMIECs, OECT devices, and bioelectronic circuits, particularly those desired for long-term applications like implantable biological sensing.

Finally, it should be reiterated that studies of OMIEC stability for OECT applications should be carried out with material sets and conditions relevant to OECT operation. Common (spectro)electrochemistry electrodes such as ITO do not reproduce the electrochemical degradation processes present in OECTs that commonly employ Au electrodes. Employing these methods to study OMIECs for OECTs may overemphasize other ultimately non-critical factors in determining device degradation. As the exact chemical species responsible for accelerated

degradation remain unclear, further study is warranted, and similar experiments should be extended to n-type OMIEC materials. Nonetheless, these results build a strong understanding of thiophene-based OMIECs popular in bioelectronics and establish the first in-depth analysis of OECT degradation. This work moves OMIECs closer to practical use in long-term applications that could benefit from the numerous advantages of OECTs, such as neural recordings, electrical stimulation, and biosensors.

ASSOCIATED CONTENT

Supporting Information.

The following files are available free of charge.

Transfer curves of p(g3T2-O) after cycling after swapping source and drain contacts; Raman spectroscopy of p(g3T2-T) after cycling in different biasing schemes; cyclic voltammetry of p(g3T2-O) during cycling; optical images of p(g3T2-O) transistor channels after cycling; differences in p(g3T2-O) degradation after source-drain shorted cycling at different scan rates; atomic force microscopy of substrates coated with p(g3T2-O) for testing; spectroelectrochemistry of p(g3T2-O) on ITO and Au-coated ITO with corresponding cyclic voltammetry before and after cycling; cyclic voltammograms on pristine films with used, basic electrolyte; grazing-incidence wide-angle x-ray scattering data of p(g3T2-O) after cyclic voltammetry cycling; transfer curves of p(g3T2-O) with self-assembled monolayer passivated gold source and drain contacts; diode-connected cycling of p(g3T2-O) while dosing with NaOH and H_2O_2 (PDF)

AUTHOR INFORMATION

Corresponding Authors

*Jonathan Rivnay & Bryan D. Paulsen – Department of Biomedical Engineering, Northwestern University, Evanston, Illinois 60208, United States; Email: jrivnay@northwestern.edu, bryan.paulsen@northwestern.edu

Author Contributions

E.A.S. and B.P. conceived the project. E.A.S., R.W., D.M., J.T., B.P., and J.R. designed and performed the experiments and analyzed the resulting data. M.M. and I.M. designed and

synthesized the conjugated polymers. E.A.S., B.P., and J.R. wrote the manuscript. All authors have given approval to the final version of the manuscript.

Notes

The authors declare no competing financial interest.

ACKNOWLEDGMENT

E.A.S. and J.R gratefully acknowledges funding support from Sloan under award no. FG-2019-12046. R.W., B.D.P., and J.R. acknowledge support from the National Science Foundation grant no. NSF DMR-1751308. E.A.S, R.W., D.M., M.M., I.M., and J.R. acknowledge funding from King Abdullah University of Science and Technology Office of Sponsored Research (OSR) under award no. OSR-2019-CRG8-4086 and OSR-2018-CRG7-3749. J. T. was primarily supported by an Office of Naval Research (ONR) Young Investigator Program (YIP) award no. N00014-20-1-2777. M.M. and I.M. acknowledge funding from ERC Synergy Grant SC2 (610115), the European Union's Horizon 2020 research and innovation program under grant agreement n°952911, project BOOSTER and grant agreement n°862474, project RoLA-FLEX, as well as EPSRC Project EP/T026219/1.This work utilized Keck-II facility of Northwestern University's NUANCE Center and Northwestern University Micro/Nano Fabrication Facility (NUFAB), which are both partially supported by Soft and Hybrid Nanotechnology Experimental (SHyNE) Resource (NSF ECCS-1542205), the Materials Research Science and Engineering Center (NSF DMR-1720139), the State of Illinois, and Northwestern University. Additionally, the Keck-II facility is partially supported by the International Institute for Nanotechnology (IIN); the Keck Foundation; and the State of Illinois, through the IIN. This research used resources of the Advanced Photon Source, a U.S. Department of Energy (DOE) Office of Science User Facility operated for the DOE Office of

Science by Argonne National Laboratory under Contract No. DE-AC02-06CH11357. Special thanks to J. Strzalka for beam line support.

References

(1) Rivnay, J.; Owens, R. M.; Malliaras, G. G. The Rise of Organic Bioelectronics. *Chem. Mater.* **2014**, *26* (1), 679–685. https://doi.org/10.1021/cm4022003.

(2) Inal, S.; Rivnay, J.; Suiu, A. O.; Malliaras, G. G.; McCulloch, I. Conjugated Polymers in Bioelectronics. *Acc. Chem. Res.* **2018**, *51* (6), 1368–1376. https://doi.org/10.1021/acs.accounts.7b00624.

(3) Paulsen, B. D.; Tybrandt, K.; Stavrinidou, E.; Rivnay, J. Organic Mixed Ionic–Electronic Conductors. *Nat. Mater.* **2020**, *19* (1), 13–26. https://doi.org/10.1038/s41563-019-0435-z.

(4) Koklu, A.; Ohayon, D.; Wustoni, S.; Druet, V.; Saleh, A.; Inal, S. Organic Bioelectronic Devices for Metabolite Sensing. *Chem. Rev.* **2021**. https://doi.org/10.1021/acs.chemrev.1c00395.

(5) Han, S.; Polyravas, A. G.; Wustoni, S.; Inal, S.; Malliaras, G. G. Integration of Organic Electrochemical Transistors with Implantable Probes. *Adv. Mater. Technol.* **2021**, *2100763*, 1–5. https://doi.org/10.1002/admt.202100763.

(6) Torricelli, F.; Adrahtas, D. Z.; Bao, Z.; Berggren, M.; Biscarini, F.; Bonfiglio, A.; Bortolotti, C. A.; Frisbie, C. D.; Macchia, E.; Malliaras, G. G.; McCulloch, I.; Moser, M.; Nguyen, T.-Q.; Owens, R. M.; Salleo, A.; Spanu, A.; Torsi, L. Electrolyte-Gated Transistors for Enhanced Performance Bioelectronics. *Nat. Rev. Methods Prim.* **2021**, *1* (66). https://doi.org/10.1038/s43586-021-00065-8.

(7) Rivnay, J.; Inal, S.; Salleo, A.; Owens, R. M.; Berggren, M.; Malliaras, G. G. Organic

Electrochemical Transistors. *Nat. Rev. Mater.* **2018**, *3*. https://doi.org/10.1038/natrevmats.2017.86.

(8) Strakosas, X.; Bongo, M.; Owens, R. M. The Organic Electrochemical Transistor for Biological Applications. *J. Appl. Polym. Sci.* **2015**, *41735*, 1–14. https://doi.org/10.1002/app.41735.

(9) Shim, N. Y.; Bernards, D. A.; Macaya, D. J.; DeFranco, J. A.; Nikolou, M.; Owens, R. M.; Malliaras, G. G. All-Plastic Electrochemical Transistor for Glucose Sensing Using a Ferrocene Mediator. *Sensors* **2009**, *9* (12), 9896–9902. https://doi.org/10.3390/s91209896.

(10) Lin, P.; Luo, X.; Hsing, I. M.; Yan, F. Organic Electrochemical Transistors Integrated in Flexible Microfluidic Systems and Used for Label-Free DNA Sensing. *Adv. Mater.* **2011**, *23* (35), 4035–4040. https://doi.org/10.1002/adma.201102017.

(11) Braendlein, M.; Pappa, A. M.; Ferro, M.; Lopresti, A.; Acquaviva, C.; Mamessier, E.; Malliaras, G. G.; Owens, R. M. Lactate Detection in Tumor Cell Cultures Using Organic Transistor Circuits. *Adv. Mater.* **2017**, *29* (13). https://doi.org/10.1002/adma.201605744.

(12) Scheiblin, G.; Coppard, R.; Owens, R. M.; Mailley, P.; Malliaras, G. G. Referenceless PH Sensor Using Organic Electrochemical Transistors. *Adv. Mater. Technol.* **2017**, *2* (2), 1–5. https://doi.org/10.1002/admt.201600141.

(13) Rivnay, J.; Ramuz, M.; Leleux, P.; Hama, A.; Huerta, M.; Owens, R. M. Organic Electrochemical Transistors for Cell-Based Impedance Sensing. *Appl. Phys. Lett.* **2015**, *106* (043301), 1–4. https://doi.org/10.1063/1.4906872.

(14) Jimison, L. H.; Tria, S. A.; Khodagholy, D.; Gurfi, M.; Lanzarini, E.; Hama, A.; Malliaras, G. G.; Owens, R. M. Measurement of Barrier Tissue Integrity with an Organic Electrochemical Transistor. *Adv. Mater.* **2012**, *24*, 5919–5923. https://doi.org/10.1002/adma.201202612.

(15) Khodagholy, D.; Doublet, T.; Quilichini, P.; Gurfinkel, M.; Leleux, P.; Ismailova, E.; Sanaur, S.; Bernard, C.; Ghestem, A.; Ismailova, E.; Herve, T.; Malliaras, G. G. In Vivo Recordings of Brain Activity Using Organic Transistors. *Nat. Commun.* **2013**, *4* (1575). https://doi.org/10.1038/ncomms2573.

(16) Gu, X.; Yeung, S. Y.; Chadda, A.; Ngar, E.; Poon, Y.; Boheler, K. R. Organic Electrochemical Transistor Arrays for In Vitro Electrophysiology Monitoring of 2D and 3D Cardiac Tissues. *Adv. Biosyst.* **2018**, *1800248*, 1–8. https://doi.org/10.1002/adbi.201800248.

(17) Cea, C.; Spyropoulos, G. D.; Jastrzebska-perfect, P.; Ferrero, J. J.; Gelinas, J. N.; Khodagholy, D. Enhancement-Mode Ion-Based Transistor as a Comprehensive Interface and Real-Time Processing Unit for in Vivo Electrophysiology. *Nat. Mater.* **2020**. https://doi.org/10.1038/s41563-020-0638-3.

(18) Williamson, A.; Ferro, M.; Leleux, P.; Ismailova, E.; Kaszas, A.; Doublet, T.; Quilichini, P.; Rivnay, J.; Rózsa, B.; Katona, G.; Bernard, C.; Malliaras, G. G. Localized Neuron Stimulation with Organic Electrochemical Transistors on Delaminating Depth Probes. *Adv. Mater.* **2015**, *27*, 4405–4410. https://doi.org/10.1002/adma.201500218.

(19) Tran, V. Van; Tran, N. H. T.; Hwang, H. S.; Chang, M. Development Strategies of

Conducting Polymer-Based Electrochemical Biosensors for Virus Biomarkers: Potential for Rapid COVID-19 Detection. *Biosens. Bioelectron.* **2021**, *182* (113192). https://doi.org/10.1016/j.bios.2021.113192.

(20) Guo, K.; Wustoni, S.; Koklu, A.; Díaz-Galicia, E.; Moser, M.; Hama, A.; Alqahtani, A. A.; Ahmad, A. N.; Alhamlan, F. S.; Shuaib, M.; Pain, A.; McCulloch, I.; Arold, S. T.; Grünberg, R.; Inal, S. Rapid Single-Molecule Detection of COVID-19 and MERS Antigens via Nanobody-Functionalized Organic Electrochemical Transistors. *Nat. Biomed. Eng.* **2021**, *5* (7), 666–677. https://doi.org/10.1038/s41551-021-00734-9.

(21) Giovannitti, A.; Rashid, R. B.; Thiburce, Q.; Paulsen, B. D.; Cendra, C.; Thorley, K.; Moia, D.; Mefford, J. T.; Hanifi, D.; Weiyuan, D.; Moser, M.; Salleo, A.; Nelson, J.; McCulloch, I.; Rivnay, J. Energetic Control of Redox-Active Polymers toward Safe Organic Bioelectronic Materials. *Adv. Mater.* **2020**, *32* (16), 1–9. https://doi.org/10.1002/adma.201908047.

(22) Veal, E. A.; Day, A. M.; Morgan, B. A. Hydrogen Peroxide Sensing and Signaling. *Mol. Cell* **2007**, *26* (1), 1–14. https://doi.org/10.1016/j.molcel.2007.03.016.

(23) Giovannitti, A.; Nielsen, C. B.; Sbircea, D. T.; Inal, S.; Donahue, M.; Niazi, M. R.; Hanifi, D. A.; Amassian, A.; Malliaras, G. G.; Rivnay, J.; McCulloch, I. N-Type Organic Electrochemical Transistors with Stability in Water. *Nat. Commun.* **2016**, *7*, 1–9. https://doi.org/10.1038/ncomms13066.

(24) Sun, H.; Vagin, M.; Wang, S.; Crispin, X.; Forchheimer, R.; Berggren, M.; Fabiano, S. Complementary Logic Circuits Based on High-Performance n-Type Organic

Electrochemical Transistors. *Adv. Mater.* **2018**, *30* (9), 1–7. https://doi.org/10.1002/adma.201704916.

(25) Luo, X.; Shen, H.; Perera, K.; Tran, D. T.; Boudouris, B. W.; Mei, J. Designing Donor-Acceptor Copolymers for Stable and High-Performance Organic Electrochemical Transistors. *ACS Macro Lett.* **2021**, *10*, 1061–1067. https://doi.org/10.1021/acsmacrolett.1c00328.

(26) Ding, B.; Kim, G.; Kim, Y.; Eisner, F. D.; Gutiérrez-Fernández, E.; Martín, J.; Yoon, M.; Heeney, M. Influence of Backbone Curvature on the Organic Electrochemical Transistor Performance of Glycolated Donor–Acceptor Conjugated Polymers. *Angew. Chemie* **2021**, *133* (36), 19831–19836. https://doi.org/10.1002/ange.202106084.

(27) Tang, K.; Miao, W.; Guo, S. Crosslinked PEDOT:PSS Organic Electrochemical Transistors on Interdigitated Electrodes with Improved Stability. *ACS Appl. Polym. Mater.* **2021**, *3* (3), 1436–1444. https://doi.org/10.1021/acsapm.0c01292.

(28) Wu, X.; Liu, Q.; Surendran, A.; Bottle, S. E.; Sonar, P.; Leong, W. L. Enhancing the Electrochemical Doping Efficiency in Diketopyrrolopyrrole-Based Polymer for Organic Electrochemical Transistors. *Adv. Electron. Mater.* **2021**, *7* (1), 1–8. https://doi.org/10.1002/aelm.202000701.

(29) Kim, S. M.; Kim, C. H.; Kim, Y.; Kim, N.; Lee, W. J.; Lee, E. H.; Kim, D.; Park, S.; Lee, K.; Rivnay, J.; Yoon, M. H. Influence of PEDOT:PSS Crystallinity and Composition on Electrochemical Transistor Performance and Long-Term Stability. *Nat. Commun.* **2018**, *9* (1). https://doi.org/10.1038/s41467-018-06084-6.

(30) Savva, A.; Ohayon, D.; Surgailis, J.; Paterson, A. F.; Hidalgo, T. C.; Chen, X.; Maria, I. P.; Paulsen, B. D.; Petty, A. J.; Rivnay, J.; McCulloch, I.; Inal, S. Solvent Engineering for High-Performance n-Type Organic Electrochemical Transistors. *Adv. Electron. Mater.* **2019**, *5* (8), 1–10. https://doi.org/10.1002/aelm.201900249.

(31) Keene, S. T.; Pol, T. P. A. Van Der; Zakhidov, D.; Weijtens, C. H. L.; Janssen, R. A. J.; Salleo, A.; Burgt, Y. Van De. Enhancement-Mode PEDOT:PSS Organic Electrochemical Transistors Using Molecular De-Doping. *Adv. Mater.* **2020**. https://doi.org/10.1002/adma.202000270.

(32) Giovannitti, A.; Rashid, R. B.; Thiburce, Q.; Paulsen, B. D.; Cendra, C.; Thorley, K.; Moia, D.; Mefford, J. T.; Hanifi, D.; Weiyuan, D.; Moser, M.; Salleo, A.; Nelson, J.; McCulloch, I.; Rivnay, J. Energetic Control of Redox-Active Polymers toward Safe Organic Bioelectronic Materials. *Adv. Mater.* **2020**, *32* (16), 1908047. https://doi.org/10.1002/ADMA.201908047.

(33) Paterson, A. F.; Savva, A.; Wustoni, S.; Tsetseris, L.; Paulsen, B. D.; Faber, H.; Emwas, A. H.; Chen, X.; Nikiforidis, G.; Hidalgo, T. C.; Moser, M.; Maria, I. P.; Rivnay, J.; McCulloch, I.; Anthopoulos, T. D.; Inal, S. Water Stable Molecular N-Doping Produces Organic Electrochemical Transistors with High Transconductance and Record Stability. *Nat. Commun.* **2020**, *11* (1), 1–11. https://doi.org/10.1038/s41467-020-16648-0.

(34) Ko, J.; Wu, X.; Surendran, A.; Muhammad, B. T.; Leong, W. L. Self-Healable Organic Electrochemical Transistor with High Transconductance, Fast Response, and Long-Term Stability. *ACS Appl. Mater. Interfaces* **2020**, *12* (30), 33979–33988. https://doi.org/10.1021/acsami.0c07913.

(35) Wu, X.; Feng, J.; Deng, J.; Cui, Z.; Wang, L.; Xie, S.; Chen, C.; Tang, C.; Han, Z.; Yu, H.; Sun, X.; Peng, H. Fiber-Shaped Organic Electrochemical Transistors for Biochemical Detections with High Sensitivity and Stability. *Sci. China Chem.* **2020**, *63* (9), 1281–1288. https://doi.org/10.1007/s11426-020-9779-1.

(36) Wu, X.; Surendran, A.; Moser, M.; Chen, S.; Muhammad, B. T.; Maria, I. P.; Mcculloch, I.; Leong, W. L. Universal Spray-Deposition Process for Scalable, High-Performance, and Stable Organic Electrochemical Transistors. *ACS Appl. Mater. Interfaces* **2020**, *12* (18), 20757–20764. https://doi.org/10.1021/acsami.0c04776.

(37) Giovannitti, A.; Sbircea, D.; Inal, S.; Nielsen, C. B.; Bandiello, E. Controlling the Mode of Operation of Organic Transistors through Side-Chain Engineering. *PNAS* **2016**, *113* (43). https://doi.org/10.1073/pnas.1608780113.

(38) Li, P.; Lei, T. Molecular Design Strategies for High-Performance Organic Electrochemical Transistors. *J. Polym. Sci.* **2021**, No. June, 1–16. https://doi.org/10.1002/pol.20210503.

(39) Zeglio, E.; Eriksson, J.; Gabrielsson, R.; Solin, N.; Inganäs, O. Highly Stable Conjugated Polyelectrolytes for Water-Based Hybrid Mode Electrochemical Transistors. *Adv. Mater.* **2017**, *29* (19). https://doi.org/10.1002/adma.201605787.

(40) Wang, N.; Xie, L.; Ling, H.; Piradi, V.; Li, L.; Wang, X.; Zhu, X.; Yan, F. Ethylenedioxythiophene Incorporated Diketopyrrolopyrrole Conjugated Polymers for High-Performance Organic Electrochemical Transistors. *J. Mater. Chem. C* **2021**, *9* (12), 4260–4266. https://doi.org/10.1039/d1tc00338k.

(41) Maria, I. P.; Paulsen, B. D.; Savva, A.; Ohayon, D.; Wu, R.; Hallani, R.; Basu, A.; Du, W.;

Anthopoulos, T. D.; Inal, S.; Rivnay, J.; McCulloch, I.; Giovannitti, A. The Effect of Alkyl Spacers on the Mixed Ionic-Electronic Conduction Properties of N-Type Polymers. *Adv. Funct. Mater.* **2021**, *31* (14). https://doi.org/10.1002/adfm.202008718.

(42) Jones, A. L.; De Keersmaecker, M.; Savagian, L. R.; DiTullio, B. T.; Pelse, I.; Reynolds, J. R. Branched Oligo(Ether) Side Chains: A Path to Enhanced Processability and Elevated Conductivity for Polymeric Semiconductors. *Adv. Funct. Mater.* **2021**, *31* (35). https://doi.org/10.1002/adfm.202102688.

(43) Krauss, G.; Meichsner, F.; Hochgesang, A.; Mohanraj, J.; Salehi, S.; Schmode, P.; Thelakkat, M. Polydiketopyrrolopyrroles Carrying Ethylene Glycol Substituents as Efficient Mixed Ion-Electron Conductors for Biocompatible Organic Electrochemical Transistors. *Adv. Funct. Mater.* **2021**, *31* (20). https://doi.org/10.1002/adfm.202010048.

(44) Wang, Y.; Hamidi-Sakr, A.; Surgailis, J.; Zhou, Y.; Liao, H.; Chen, J.; Zhu, G.; Li, Z.; Inal, S.; Yue, W. The Effect of the Donor Moiety of DPP Based Polymers on the Performance of Organic Electrochemical Transistors. *J. Mater. Chem. C* **2021**, *9* (38), 13338–13346. https://doi.org/10.1039/d1tc02994k.

(45) Ohayon, D.; Savva, A.; Du, W.; Paulsen, B. D.; Uguz, I.; Ashraf, R. S.; Rivnay, J.; McCulloch, I.; Inal, S. Influence of Side Chains on the N-Type Organic Electrochemical Transistor Performance. *ACS Appl. Mater. Interfaces* **2021**, *13* (3), 4253–4266. https://doi.org/10.1021/acsami.0c18599.

(46) Jia, H.; Huang, Z.; Li, P.; Zhang, S.; Wang, Y.; Wang, J. Y.; Gu, X.; Lei, T. Engineering Donor-Acceptor Conjugated Polymers for High-Performance and Fast-Response Organic

Electrochemical Transistors. *J. Mater. Chem. C* **2021**, *9* (14), 4927–4934. https://doi.org/10.1039/d1tc00440a.

(47) Feng, K.; Shan, W.; Ma, S.; Wu, Z.; Chen, J.; Guo, H.; Liu, B.; Wang, J.; Li, B.; Woo, H. Y.; Fabiano, S.; Huang, W.; Guo, X. Fused Bithiophene Imide Dimer-Based N-Type Polymers for High-Performance Organic Electrochemical Transistors. *Angew. Chemie* **2021**, *133* (45), 24400–24407. https://doi.org/10.1002/ange.202109281.

(48) Zeglio, E.; Schmidt, M. M.; Thelakkat, M.; Gabrielsson, R.; Solin, N.; Inganäs, O. Conjugated Polyelectrolyte Blends for Highly Stable Accumulation-Mode Electrochemical Transistors. *Chem. Mater.* **2017**, *29* (10), 4293–4300. https://doi.org/10.1021/acs.chemmater.7b00474.

(49) Giovannitti, A.; Thorley, K. J.; Nielsen, C. B.; Li, J.; Donahue, M. J.; Malliaras, G. G.; Rivnay, J.; McCulloch, I. Redox-Stability of Alkoxy-BDT Copolymers and Their Use for Organic Bioelectronic Devices. *Adv. Funct. Mater.* **2018**, *28* (17). https://doi.org/10.1002/adfm.201706325.

(50) Wang, Y.; Zeglio, E.; Liao, H.; Xu, J.; Liu, F.; Li, Z.; Maria, I. P.; Mawad, D.; Herland, A.; Mcculloch, I.; Yue, W. Hybrid Alkyl-Ethylene Glycol Side Chains Enhance Substrate Adhesion and Operational Stability in Accumulation Mode Organic Electrochemical Transistors. *Chem. Mater.* **2019**, *31* (23), 9797–9806. https://doi.org/10.1021/acs.chemmater.9b03798.

(51) Bischak, C. G.; Flagg, L. Q.; Yan, K.; Li, C. Z.; Ginger, D. S. Fullerene Active Layers for N-Type Organic Electrochemical Transistors. *ACS Appl. Mater. Interfaces* **2019**, *11* (31),

28138–28144. https://doi.org/10.1021/acsami.9b11370.

(52) Moser, M.; Hidalgo, T. C.; Surgailis, J.; Gladisch, J.; Ghosh, S.; Sheelamanthula, R.; Thiburce, Q.; Giovannitti, A.; Salleo, A.; Gasparini, N.; Wadsworth, A.; Zozoulenko, I.; Berggren, M.; Stavrinidou, E.; Inal, S.; McCulloch, I. Side Chain Redistribution as a Strategy to Boost Organic Electrochemical Transistor Performance and Stability. *Adv. Mater.* **2020**, *32* (37). https://doi.org/10.1002/adma.202002748.

(53) Kim, J. H.; Ahmad, Z.; Kim, Y.; Kim, W.; Ahn, H.; Lee, J. S.; Yoon, M. H. Decoupling Critical Parameters in Large-Range Crystallinity-Controlled Polypyrrole-Based High-Performance Organic Electrochemical Transistors. *Chem. Mater.* **2020**, *32* (19), 8606–8618. https://doi.org/10.1021/acs.chemmater.0c02936.

(54) Chen, X.; Marks, A.; Paulsen, B. D.; Wu, R.; Rashid, R. B.; Chen, H.; Alsufyani, M.; Rivnay, J.; McCulloch, I. N-Type Rigid Semiconducting Polymers Bearing Oligo(Ethylene Glycol) Side Chains for High-Performance Organic Electrochemical Transistors. *Angew. Chemie - Int. Ed.* **2021**, *60* (17), 9368–9373. https://doi.org/10.1002/anie.202013998.

(55) Moser, M.; Savva, A.; Thorley, K.; Paulsen, B. D.; Hidalgo, T. C.; Ohayon, D.; Chen, H.; Giovannitti, A.; Marks, A.; Gasparini, N.; Wadsworth, A.; Rivnay, J.; Inal, S.; McCulloch, I. Polaron Delocalization in Donor–Acceptor Polymers and Its Impact on Organic Electrochemical Transistor Performance. *Angew. Chemie - Int. Ed.* **2021**, *60* (14), 7777–7785. https://doi.org/10.1002/anie.202014078.

(56) Szumska, A. A.; Maria, I. P.; Flagg, L. Q.; Savva, A.; Surgailis, J.; Paulsen, B. D.; Moia, D.; Chen, X.; Griggs, S.; Mefford, J. T.; Rashid, R. B.; Marks, A.; Inal, S.; Ginger, D. S.;

Giovannitti, A.; Nelson, J. Reversible Electrochemical Charging of N-Type Conjugated Polymer Electrodes in Aqueous Electrolytes. *J. Am. Chem. Soc.* **2021**, *143* (36), 14795–14805. https://doi.org/10.1021/jacs.1c06713.

(57) Park, S.; Kim, S. H.; Choi, H. H.; Kang, B.; Cho, K. Recent Advances in the Bias Stress Stability of Organic Transistors. *Adv. Funct. Mater.* **2020**, *30* (20). https://doi.org/10.1002/adfm.201904590.

(58) Iqbal, H. F.; Ai, Q.; Thorley, K. J.; Chen, H.; McCulloch, I.; Risko, C.; Anthony, J. E.; Jurchescu, O. D. Suppressing Bias Stress Degradation in High Performance Solution Processed Organic Transistors Operating in Air. *Nat. Commun.* **2021**, *12* (1), 1–10. https://doi.org/10.1038/s41467-021-22683-2.

(59) Flagg, L. Q.; Bischak, C. G.; Onorato, J. W.; Rashid, R. B.; Luscombe, C. K.; Ginger, D. S. Polymer Crystallinity Controls Water Uptake in Glycol Side Chain Polymer Organic Electro- Chemical Transistors. *J. Am. Chem. Soc.* **2019**. https://doi.org/10.1021/jacs.8b12640.

(60) Nielsen, C. B.; Giovannitti, A.; Sbircea, D.-T.; Bandiello, E.; Niazi, M. R.; Hanifi, D. A.; Sessolo, M.; Amassian, A.; Malliaras, G. G.; Rivnay, J.; McCulloch, I. Molecular Design of Semiconducting Polymers for High-Performance Organic Electrochemical Transistors. *J. Am. Chem. Soc.* **2016**, *138* (32), 10252–10259. https://doi.org/10.1021/JACS.6B05280.

(61) Venkatraman, V.; Friedlein, J. T.; Giovannitti, A.; Maria, I. P.; Mcculloch, I.; Mcleod, R. R.; Rivnay, J. Subthreshold Operation of Organic Electrochemical Transistors for Biosignal Amplification. *Adv. Sci. News* **2018**, *1800453*, 1–7.

https://doi.org/10.1002/advs.201800453.

(62) Francis, C.; Fazzi, ab D.; Grimm, S. B.; Paulus, F.; Beck, S.; Hillebrandt, de S.; Pucci de, de A.; Zaumseil, J. Raman Spectroscopy and Microscopy of Electrochemically and Chemically Doped High-Mobility Semiconducting Polymers †. *J. Mater. Chem. C* **2017**, *5*, 6176. https://doi.org/10.1039/c7tc01277b.

(63) Wada, Y.; Enokida, I.; Yamamoto, J.; Furukawa, Y. Raman Imaging of Carrier Distribution in the Channel of an Ionic Liquid-Gated Transistor Fabricated with Regioregular Poly(3-Hexylthiophene). *Spectrochim. Acta Part A Mol. Biomol. Spectrosc.* **2018**, *197*, 166–169. https://doi.org/10.1016/J.SAA.2018.01.043.

(64) Moser, M.; Savagian, L. R.; Savva, A.; Matta, M.; Ponder, J. F.; Hidalgo, T. C.; Ohayon, D.; Hallani, R.; Reisjalali, M.; Troisi, A.; Wadsworth, A.; Reynolds, J. R.; Inal, S.; McCulloch, I. Ethylene Glycol-Based Side Chain Length Engineering in Polythiophenes and Its Impact on Organic Electrochemical Transistor Performance. *Chem. Mater.* **2020**, *32* (15), 6618–6628. https://doi.org/10.1021/acs.chemmater.0c02041.

(65) Cendra, C.; Giovannitti, A.; Savva, A.; Venkatraman, V.; McCulloch, I.; Salleo, A.; Inal, S.; Rivnay, J. Role of the Anion on the Transport and Structure of Organic Mixed Conductors. *Adv. Funct. Mater.* **2019**, *29* (5), 1–11. https://doi.org/10.1002/adfm.201807034.

(66) Paulsen, B. D.; Giovannitti, A.; Wu, R.; Strzalka, J.; Zhang, Q.; Rivnay, J.; Takacs, C. J. Electrochemistry of Thin Films with In Situ/Operando Grazing Incidence X-Ray Scattering: Bypassing Electrolyte Scattering for High Fidelity Time Resolved Studies. *Small* **2021**, *17*

(42), 1–7. https://doi.org/10.1002/smll.202103213.

(67) Bischak, C. G.; Flagg, L. Q.; Yan, K.; Rehman, T.; Davies, D. W.; Quezada, R. J.; Onorato, J. W.; Luscombe, C. K.; Diao, Y.; Li, C. Z.; Ginger, D. S. A Reversible Structural Phase Transition by Electrochemically-Driven Ion Injection into a Conjugated Polymer. *J. Am. Chem. Soc.* **2020**, *142* (16), 7434–7442. https://doi.org/10.1021/jacs.9b12769.

(68) Benck, J. D.; Pinaud, B. A.; Gorlin, Y.; Jaramillo, T. F. Substrate Selection for Fundamental Studies of Electrocatalysts and Photoelectrodes: Inert Potential Windows in Acidic, Neutral, and Basic Electrolyte. *PLoS One* **2014**, *9* (10). https://doi.org/10.1371/journal.pone.0107942.

(69) Hayyan, M.; Hashim, M. A.; Alnashef, I. M. Superoxide Ion: Generation and Chemical Implications. *Chem. Rev.* **2016**, *116* (5), 3029–3085. https://doi.org/10.1021/ACS.CHEMREV.5B00407.

(70) Cao, H.; Rupar, P. A. Recent Advances in Conjugated Furans. *Chem. - A Eur. J.* **2017**, *23* (59), 14670–14675. https://doi.org/10.1002/chem.201703355.

(71) Amanchukwu, C. V.; Gauthier, M.; Batcho, T. P.; Symister, C.; Shao-Horn, Y.; D'Arcy, J. M.; Hammond, P. T. Evaluation and Stability of PEDOT Polymer Electrodes for Li-O2 Batteries. *J. Phys. Chem. Lett.* **2016**, *7* (19), 3770–3775. https://doi.org/10.1021/acs.jpclett.6b01986.

(72) Park, J. K.; Lee, S. Sulfoxide and Sulfone Synthesis via Electrochemical Oxidation of Sulfides. *J. Org. Chem.* **2021**, *86*, 13790–13799. https://doi.org/10.1021/acs.joc.1c01657.

(73) Jiang, T.; Malone, W.; Tong, Y.; Dragoe, D.; Bendounan, A.; Kara, A.; Esaulov, V. A. Thiophene Derivatives on Gold and Molecular Dissociation Processes. *J. Phys. Chem. C* **2017**, *121* (50), 27923–27935. https://doi.org/10.1021/acs.jpcc.7b08006.

For Table of Contents Only: